

Catalytic oxidative dehydrogenation of propane over Mg–V/Mo oxides

Jason D. Pless,^a Billy B. Bardin,^b Hack-Sung Kim,^a Donggeun Ko,^{a,c} Matthew T. Smith,^b
Robin R. Hammond,^b Peter C. Stair,^a and Kenneth R. Poeppelmeier^{a,*}

^a Department of Chemistry, Institute for Environmental Catalysis, Northwestern University, 2145 Sheridan Road, Evanston, IL 60208-3113, USA

^b The Dow Chemical Company, 3200 Kanawha Turnpike, South Charleston, WV, 25303, USA

^c Research and Development Center, Rubicon Technology Inc., Bannockburn, IL 60015, USA

Received 13 October 2003; revised 15 January 2004; accepted 22 January 2004

Abstract

Fifteen distinct MgO–V₂O₅, MgO–MoO₃, MgO–V₂O₅–MoO₃, and V₂O₅–MoO₃ compositions were prepared using sol–gel chemistry and their selectivities and conversions for propane oxidative dehydrogenation (ODH) to propylene were measured. The vanadates were more active than the molybdates at lower temperatures; however, the molybdates exhibited higher selectivities at similar conversions. An increase in both ODH conversion and selectivity with molybdenum substitution on vanadium sites was also observed. These results demonstrate the importance of the bulk structure on the ODH reaction. In general, propylene selectivities increased with increasing conversions at temperatures above 673 K when oxygen depletion in the reactant stream occurred. Visible and UV Raman spectroscopy corroborates this result and helps focus attention on critical surface-specific information. A new Raman peak was observed for the partially reduced MgMoO₄ and is associated with a three-coordinate surface oxygen.

© 2004 Elsevier Inc. All rights reserved.

Keywords: Propane; Oxidative dehydrogenation; ODH; Magnesium, vanadium, and molybdenum oxides; Raman spectroscopy

1. Introduction

The selective conversion of short chain alkanes (C₃H₈–C₅H₁₂) to useful intermediates via catalytic oxidative dehydrogenation (ODH) is of interest to the petrochemical and energy industries and has been studied extensively [1–6]. The oxidative dehydrogenation of propane to propylene has been studied using vanadium- and molybdenum-oxide-based catalysts [7–17]. The reaction is believed to proceed by a Mars–van Krevelen reaction mechanism [18–24], in which adsorbed propane reacts with lattice oxygen and the reduced metal oxide reacts with adsorbed, dissociated O₂ [25]. A fundamental understanding of the active surface(s) and the reaction mechanism is needed to improve the selectivity and conversion of propane ODH and increase the yield of propylene.

Magnesium vanadium oxide catalysts have received considerable attention for the ODH of propane [6–12,26–29]. It is generally accepted that the reaction proceeds by the abstraction of a hydrogen from the alkane and reduction

of a tetrahedrally coordinated V⁵⁺ species [26]. Magnesium orthovanadate, Mg₃(VO₄)₂, contains isolated VO₄^{3–} anions [30], and the pyrovanadate, Mg₂V₂O₇, is composed of corner-shared VO₄ tetrahedra in the V₂O₇^{4–} units [31]. However, the specific structure of the active site is unknown. Kung and co-workers attribute the selectivity for propylene to the Mg₃(VO₄)₂ structure, and suggest that the oxygen atoms in the V–O–Mg bonds are harder to reduce than the bridging oxygen in the V–O–V bonds in Mg₂V₂O₇ [28,29]. In contrast, Volta and co-workers report that Mg₂V₂O₇ is the selective phase and Mg₃(VO₄)₂ leads to the complete oxidation of the alkanes [8]. They relate the selectivity with the ability of the corner-shared VO₄ tetrahedra in the V₂O₇^{4–} anion to stabilize V⁴⁺ associated with an oxygen vacancy [27]. Conversely, Fang et al. state that Mg₃(VO₄)₂ exhibits a higher conversion, but Mg₂V₂O₇ is more selective at the same conversions [12]. These discrepancies in the catalytic properties generally are attributed to differences in preparation methods [9,28,32].

Several authors have demonstrated that magnesium molybdates exhibit higher selectivities but lower activities compared to those of the magnesium vanadates [14,15,33–36]. Interestingly, each of these reports describes an improve-

* Corresponding author.

E-mail address: krp@northwestern.edu (K.R. Poeppelmeier).

ment in the catalytic activity of MgMoO_4 with a slight excess of molybdenum oxide. Cadus and co-workers conclude that a synergistic effect between MgMoO_4 and MoO_3 results in the enhanced activity [35]. They relate the effect to a modification of the active sites of the two phase MgMoO_4 – MoO_3 catalyst [35]. Similarly, Lee et al. attribute the improved activity to MoO_x clusters on the surface of MgMoO_4 [36]. Their conclusion is based on studies of MoO_3 supported on “inactive” MgMoO_4 and treatments of MgMoO_4 with acid and base solutions to modify their surfaces [36]. In contrast, Miller et al. assign the increased activity to the formation of MgMo_2O_7 [17], which forms from the reaction of MoO_3 and MgMoO_4 .

The three phases, $\text{Mg}_2\text{V}_2\text{O}_7$, $\text{Mg}_3(\text{VO}_4)_2$, and MgMoO_4 , have been shown to be active and selective for the ODH of propane; therefore, the more complex MgO – V_2O_5 – MoO_3 system should contain interesting ODH catalysts. Previously, Harding and co-workers investigated the phase equilibria of MgO – V_2O_5 – MoO_3 and reported the discovery of two new features: a new compound $\text{Mg}_{2.5}\text{VMoO}_8$ and molybdenum substitution into magnesium orthovanadate, $\text{Mg}_{3-x}(\text{V}_{1-x}\text{Mo}_x\text{O}_4)_2$, $\sim 0.03 > x > 0$ [37]. The authors state that molybdenum substitutes into both crystal lattices, such that the oxidation state of vanadium remains unchanged; electrical neutrality is maintained by the presence of magnesium vacancies. Wang et al. report considerable substitution of vanadium and molybdenum into the $\text{Mg}_{2.5}\text{VMoO}_8$ structure, $\text{Mg}_{2.5+x}\text{V}_{1+2x}\text{Mo}_{1-2x}\text{O}_8$ ($-0.05 \leq x \leq 0.05$) [38]. Zubkov and co-workers emphasize a third, interesting aspect in the ternary phase diagram, the coexistence of the solid solution $\text{V}_{2-2x}\text{Mo}_{2x}\text{O}_{5+x}$, $\sim 0.15 > x > 0$ with MgMoO_4 [39]. This result suggests that MgMoO_4 can serve as a support for $\text{V}_{2-2x}\text{Mo}_{2x}\text{O}_{5+x}$.

The mixing of the constituent oxides, competitive side reactions, and/or the presence of trace impurities can complicate the preparation of single-phase catalyst samples. Catalysts have been prepared by impregnation techniques [8,9,15,26,34], or the reaction of metal solutions stabilized at contrasting pH [14,16,17], which can lead one of the metal species to preferentially precipitate from solution. Generally, single-phase mixed metal oxides form at high calcination temperatures (> 973 K), but the samples have low surface areas [8]. Calcinations at lower temperatures often result in incomplete reactions and a mixture of phases [8,9,14,17]. In this study, a series of mixed metal oxides in the MgO – V_2O_5 – MoO_3 ternary system were prepared for the first time, to the best of our knowledge, by a sol–gel method. In general, the sol–gel method allows single-phase samples to be synthesized at lower temperatures (823 K) because of the intimate and nearly homogeneous mixing of the constituent elements. The lower reaction temperatures result in a smaller average particle size and an increased surface area.

Catalyst structure may depend on the conditions under which the sample has been characterized [40–45], therefore it is important to study the structure of a catalyst under conditions that replicate the reaction conditions. Such

in situ characterization might provide insight into the reaction mechanism(s) that occur(s) during the applied reaction conditions. Raman spectroscopy recently has been applied successfully to examine catalysts during reaction conditions [43,44,46–48].

The present work is directed toward understanding the reaction pathway of propane ODH on the catalyst surface. We report the novel synthesis of compositions found in the MgO – V_2O_5 – MoO_3 ternary system and compare their selectivities and conversions for the propane ODH. Raman spectroscopy was used to characterize the (surface) structures of $\text{Mg}_3(\text{VO}_4)_2$ and MgMoO_4 during replicated reaction conditions. These results are related to the ODH selectivities and conversions.

2. Experimental

Fifteen catalysts found in the MgO – V_2O_5 , MgO – V_2O_5 – MoO_3 , MgO – MoO_3 , and V_2O_5 – MoO_3 systems were prepared by a sol–gel technique (Table 1). Stoichiometric amounts of magnesium ethoxide (Mg 21–22%, Alfa Aesar), vanadium triisopropoxide oxide (95–99%, Alfa Aesar), and bis(acetylacetonato)dioxomolybdenum(VI) (99%, Aldrich) were dissolved in 2-methoxy ethanol (99%, Aldrich) and refluxed. An appropriate amount of a 5% by volume NH_4OH aqueous solution was added so that four equivalents of water were present for every –OR group. This ensured hydrolysis of the alkoxide groups. Upon hydrolysis, the sample precipitated from solution. After evaporation of the solvent at 383 K, the samples were calcined in a flow of O_2 for 12 h at 823 K. Higher reaction temperatures (up to 1273 K) were required to synthesize the three $\text{Mg}_{2.5+x}\text{V}_{1+2x}\text{Mo}_{1-2x}\text{O}_8$ ($x = -0.04, 0, \text{ and } 0.04$) compounds (respectively, **E**, **F**, and **G**). A 1:2 molar mixture of $\text{Mg}_3(\text{VO}_4)_2/\text{MgMoO}_4$ (**H**) was prepared to compare its catalytic properties with those of $\text{Mg}_{2.5}\text{VMoO}_8$ (**F**). The $\text{V}_{2-2x}\text{Mo}_{2x}\text{O}_{5+x}$ ($x = 0, 0.07, \text{ and } 0.14$)-supported catalysts (respectively, **L**, **M**, and **N**) were synthesized by first preparing the MgMoO_4 support by the above procedures. After calcination, the support was impregnated with stoichiometric amounts of the alkoxides for a 2% by molarity $\text{V}_{2-2x}\text{Mo}_{2x}\text{O}_{5+x}$ ($x = 0, 0.07, \text{ and } 0.14$) and the samples were recalcined for 12 h at 823 K.

A reference sample of $\text{Mg}_2\text{V}_2\text{O}_7$ (Table 1, footnote c) was prepared by a solid-state ceramic technique to compare its particle size with the sol–gel prepared $\text{Mg}_2\text{V}_2\text{O}_7$ (**B**). Stoichiometric amounts of MgO (99.95%, Alfa Aesar) and V_2O_5 (99.6+%, Aldrich) were combined and the metal oxides were mixed using an agate mortar and pestle. Ethanol was added to help achieve an intimate mixture. The sample was calcined in a flow of O_2 for 12 h at 873 K.

X-ray diffraction (XRD) patterns of the polycrystalline samples were recorded at room temperature on a Rigaku diffractometer (Cu- K_α radiation, Ni filter, 40 kV, 20 mA; $2\theta = 10$ – 70° , 0.05° step size, and 1-s count time). The crystalline phases were identified by comparison with the data

Table 1
Physical properties of metal oxides in the MgVO, MgMoO, MgVMoO, and VMoO systems

Ref. ^a label	Targeted formulation	Calcination temperature (K)	Structure of fresh catalyst (by XRD)	PDF ^b Ref. card	Surface area (m ² g ⁻¹)	Physical appearance of fresh catalyst
A	MgV ₂ O ₆ (meta)	823	MgV ₂ O ₆	45-1050	4.3	Light yellow
B	Mg ₂ V ₂ O ₇ (pyro) ^c	823	α-Mg ₂ V ₂ O ₇	31-0816	9.0	Off white
C	Mg ₃ (VO ₄) ₂ (ortho)	823	Mg ₃ (VO ₄) ₂	37-0351	29.3	Off white
D	Mg _{2.98} (V _{0.98} Mo _{0.02} O ₄) ₂	823	Mg ₃ (VO ₄) ₂	37-0351	26.5	Dull yellow
E	Mg _{2.54} V _{1.08} Mo _{0.92} O ₈	1223	Mg _{2.5} VMoO ₈	82-2074	0.91	White
F	Mg _{2.5} VMoO ₈	1173	Mg _{2.5} VMoO ₈	82-2074	0.62	Dull yellow
G	Mg _{2.46} V _{0.92} Mo _{1.08} O ₈	1323	Mg _{2.5} VMoO ₈	82-2074	0.29	Dull yellow
H	1:2 molar ratio Mg ₃ V ₂ O ₈ /MgMoO ₄	823	Mg ₃ (VO ₄) ₂ / β-MgMoO ₄	37-0351 72-2153	28.0	Off white
I	Mg _{0.992} MoO _{3.992} ^d	823	β-MgMoO ₄	72-2153	4.2	Pale gray
J	Mg _{1.015} MoO _{4.015} ^e	823	β-MgMoO ₄	72-2153	11.1	White
K	MgMo ₂ O ₇	823	MgMo ₂ O ₇	32-0622	2.4	White
L	2% V ₂ O ₅ /MgMoO ₄	823	β-MgMoO ₄ / V ₂ O ₅	72-2153 41-1426	4.0	Pale gray
M	0.14% MoO ₃ / 1.86% V ₂ O ₅ / MgMoO ₄	823	β-MgMoO ₄ / V ₂ O ₅	72-2153 41-1426	3.8	Pale gray
N	0.28% MoO ₃ / 1.72% V ₂ O ₅ / MgMoO ₄	823	β-MgMoO ₄ / V ₂ O ₅	72-2153 41-1426	3.9	Pale gray
O	MoV ₂ O ₈	823	MoV ₂ O ₈ / V ₂ O ₅	74-1510 41-1426	2.2	Brown

^a **A–D** are MgVO, **E–H** are MgVMoO, **J–K** are MgMoO, **L–N** are VMoO supported on MgMoO, and **O** is VMoO.

^b Powder diffraction file reported in the JCPDS (Joint Committee of Powder Diffraction Standards) database.

^c A single-phase sample was prepared by the solid-state technique and had a surface area of 1.1 m² g⁻¹.

^d XRD indicates single-phase sample; however, the sample is likely to consist of a mixture of MgMoO₄ and MoO₃.

^e XRD indicates single-phase sample; however, the sample is likely to consist of a mixture of MgMoO₄ and Mg(OH)₂.

reported in the JCPDS (Joint Committee of Powder Diffraction Standards) database.

Thermal gravimetric analysis (TGA) was performed on the Mg₃(VO₄)₂ sol–gel precipitate in flowing oxygen to study the combustion of the residual alkoxide moieties during calcination. Measurements were made on a TA Instruments TGA 2950 thermogravimetric analyzer. The heating profile was a linear ramp from room temperature to 723 K at 2 K min⁻¹. The sample was held isothermally at 723 K for 12 h and then heated to 923 K at 2 K min⁻¹.

Surface areas were measured by N₂ adsorption at 77 K using an OMNISORP 360 and determined using a 5-point Brunauer, Emmet, and Teller (BET) method. Krypton adsorption measurements, using a Micromeritics ASAP (Accelerated Surface Area and Porosimetry) 2405 Instrument at 77 K, were made for the accurate determination of surface areas that were < 1 m² g⁻¹.

Scanning electron microscopy (SEM) micrographs of Mg₂V₂O₇ prepared by the solid-state technique, and Mg₂V₂O₇ (**B**) and Mg₃(VO₄)₂ (**C**) prepared by the sol–gel method, were obtained with a Hitachi S-4500 FE-SEM. Samples were deposited on carbon tape and coated with 5 nm of gold to prevent charging.

Inductively coupled plasma-atomic emission spectrophotometry (ICP-AES, Thermo Jarrell Ash Atomscan Model 25 Sequential ICP spectrometer) was used to determine the Mg/Mo atomic ratios in the magnesium molybdate samples

(**I** and **J**). Approximately 0.1 g samples were dissolved with 6 ml of 15.8 M HNO₃ and diluted to ~ 20 μg ml⁻¹ of solution. The samples were further diluted to ~ 1 μg ml⁻¹ of solution to inspect for possible contaminants using inductively coupled plasma-mass spectroscopy (ICP-MS).

Visible Raman spectra were obtained for the sol–gel prepared Mg₂V₂O₇ (**B**), Mg₃(VO₄)₂ (**C**), Mg_{2.98}(V_{0.98}Mo_{0.02}O₄)₂ (**D**), 1/2 molar mixture Mg₃(VO₄)₂/MgMoO₄ (**H**), Mg_{0.992}MoO_{3.992} (**I**), and Mg_{1.015}MoO_{4.015} (**J**). The metal oxides were sieved to 60/140 mesh particles and ~ 0.5 cm of material was packed and centered into a ~ 2-cm-long quartz tube (i.d., 3.0 mm; o.d., 5.0 mm). Samples were loaded into a high-pressure cell and translated laterally to minimize laser-induced damage. The spectra were collected using ~ 60 mW of 514.5 nm radiation of a Lexel Model 95 Argon ion laser, and a SPEX triplemate spectrograph equipped with a CCD detector. An acetaminophen standard was used as a reference to calibrate the spectra. In addition, visible Raman spectroscopy characterized the structures of Mg₃(VO₄)₂ (**C**) and Mg_{0.992}MoO_{3.992} (**I**) during replicated reaction conditions. The samples were exposed to reaction gas (30% C₃H₈, 10% O₂, and 60% N₂ by volume) flowing at 50 standard cm³ min⁻¹ (sccm, ml min⁻¹) while the spectra were taken at 303, 623, 673, 723, and 798 K. Then, the samples were reoxidized at 798 K with flowing air while the spectra were taken. Spectra of fresh samples were collected while heating at 798 K in a 100 sccm flow of He.

Table 2
Oxidative dehydrogenation of propane over magnesium vanadates and molybdates^a

Ref. label	Targeted formulation	Mass tested (g)	5% conversion ^b		10% conversion ^b		High conversion ^c		
			Selectivity (%)	Temperature (K)	Selectivity (%)	Temperature (K)	Temperature (K)	Conversion (%)	Selectivity (%)
A	MgV ₂ O ₆ (meta)	2.07	57.2	626	44.2	661	811	15.2	47.6
B	Mg ₂ V ₂ O ₇ (pyro)	1.67	54.5	638	47.4	671	807	15.6	53.1
C	Mg ₃ V ₂ O ₈ (ortho)	1.70	23.4	641	29.1	698	807	12.6	40.3
D	Mg _{2.98} V _{1.08} Mo _{0.02} O ₄) ₂	1.71	46.0	623	40.6	652	804	16.5	55.6
E	Mg _{2.54} V _{1.08} Mo _{0.92} O ₈	2.28	–	–	–	–	807	4.6	38.4
F	Mg _{2.5} VMoO ₈	2.64	45.2	806	–	–	808	5.4	40.2
G	Mg _{2.46} V _{0.92} Mo _{1.08} O ₈	2.75	57.4	763	46.8	806	809	10.4	46.0
H	1:2 Mg ₃ V ₂ O ₈ /MgMoO ₄	1.56	29.7	702	30.8	738	806	13.2	40.5
I	Mg _{0.992} MoO _{3.992}	2.30	76.8	690	71.3	724	808	18.6	61.8
J	Mg _{1.015} MoO _{4.015}	2.01	46.0	731	44.6	742	806	15.4	49.2
K	MgMo ₂ O ₇	2.53	70.7	678	61.3	714	798	17.3	58.8
L	2% V ₂ O ₅ /MgMoO ₄	2.34	59.6	678	54.1	718	813	16.8	59.3
M	0.14% MoO ₃ /1.86% V ₂ O ₅ /MgMoO ₄	2.44	61.1	673	47.4	707	813	18.2	60.5
N	0.28% MoO ₃ /1.72% V ₂ O ₅ /MgMoO ₄	2.33	66.2	677	52.0	710	814	17.8	60.4
O	MoV ₂ O ₈	2.82	35.2	620	17.1	676	811	12.9	35.5
	Quartz chips	–	–	–	–	–	808	3.3	51.1

^a Test conditions: 30% C₃H₈, 10% O₂ (50 psig, 4000 GHSV, total flow = 133 sccm 14/30 mesh catalyst). Conversion and selectivity computed based on gas-phase components only.

^b Interpolated from the observed data.

^c Highest conversion obtained.

UV Raman spectroscopy characterized Mg₃(VO₄)₂ (**C**) and Mg_{0.992}MoO_{3.992} (**I**) after they were exposed to replicated reaction conditions. The UV Raman spectra were collected using ~ 5 mW of the 244 nm line, which was generated by frequency doubling the 488 nm output of an Ar⁺ ion laser to 244 nm using a temperature-tuned BBO (β -BaB₂O₄) crystal. The Raman scatterings from the samples were collected using an ellipsoidal mirror, in an 180° back-scattering geometry, coated with Al:MgF₂ to improve UV reflectivity. The photons were focused onto a Spex triple-grating spectrometer equipped with an imaging photomultiplier tube. The spectral resolution is limited by the detector to ~ 20 cm⁻¹. Standards of chloroform, cyclohexane, ethyl acetate, and Teflon were used to calibrate the spectra. One-gram samples were placed into a fluidized bed cell [49]. The samples were exposed to a 30 sccm flow of reaction gas (75% C₃H₈ and 25% O₂ by volume) for 1 h at 303, 623, 673, 723, and 798 K. Then, the samples were reoxidized with a 7.5 sccm flow of O₂ for 1 h at 798 K. In addition, spectra were collected after heating fresh samples at 798 K for 1 h in a 25 sccm flow of He. All samples were cooled to 298 K before the UV Raman spectra were taken under flowing N₂ for 1 h. This procedure was adopted to protect the ellipsoidal mirror from heat damage.

The selectivities and conversions of the metal oxides were measured for the oxidative dehydrogenation of propane. Catalyst powders were pressed at 1020 atm for 15 min to form a 3.18-cm-diameter tablet. The tablet was then crushed and sieved to 14/30 mesh particles. Propane ODH conversions and selectivities were tested in a packed bed, down-

flow reactor using 2 cm³ of catalyst. The catalyst was diluted with 2 cm³ of quartz chips (14/30 mesh) to prevent the formation of temperature gradients. A reactant gas mixture of 39.9 sccm C₃H₈, 13.3 sccm O₂, and 79.8 sccm N₂ was introduced into the reactor at 3.4 atm. The reactor was heated to 573 K, data were collected after 3 h, and then the temperature was increased by 25 K. Again, the data were collected after the reaction proceeded for 3 h. This procedure was repeated until data had been collected every 25 to 773 K with a final 35 K increase to 808 K, where the temperature was held for 24 h and data were collected every 3 h. In all studies, the reactor effluent passed through a condenser to remove water and liquid oxygenated products. Gas-phase reactants and products were analyzed with an on-line HP 6890 gas chromatograph equipped with a thermal conductivity detector. Chromatograph separation was accomplished with a molecular sieve column, a Poroplot Q, and an alumina/KCl column. The condensate was analyzed offline with an HP5890 Series II chromatograph using a Supelcowax column and a flame ionization detector. The conversions and selectivities listed in Table 2 are based on carbon and are calculated by the following equations:

$$\text{Conversion} = \left(\frac{(3 * [\text{C}_3\text{H}_6] + [\text{CO}] + [\text{CO}_2])}{(3 * [\text{C}_3\text{H}_8]_{\text{reactant}})} \right) * 100\%$$

$$\text{Selectivity} = \left(\frac{(3 * [\text{C}_3\text{H}_6])}{(3 * [\text{C}_3\text{H}_6] + [\text{CO}] + [\text{CO}_2])} \right) * 100\%$$

3. Results and discussion

3.1. Catalyst synthesis and characterization

Metal oxides were synthesized at 823 K by the sol–gel method and analyzed with powder X-ray diffraction (XRD) (Fig. 1). Examination of the powder diffraction patterns reveals the formation of the targeted compositions without the presence of trace impurities with a few exceptions. The MoV_2O_8 (**O**) and the three $\text{Mg}_{2.5+x}\text{V}_{1+2x}\text{Mo}_{1-2x}\text{O}_8$ compositions (**E**, **F**, and **G**) were not single-phase samples at 823 K. The diffraction pattern for **O** contains peaks indicative of V_2O_5 . It has been reported that the preparation method and the calcination temperature influence the composition of Mo–V oxides [50–52]. The $\text{Mg}_{2.5+x}\text{V}_{1+2x}\text{Mo}_{1-2x}\text{O}_8$ structure is located along the $\text{Mg}_3(\text{VO}_4)_2$ – MgMoO_4 tie line. A mixture of $\text{Mg}_3(\text{VO}_4)_2$ and MgMoO_4 is present at 823 K because the $\text{Mg}_{2.5}\text{VMoO}_8$ -type structure does not form appreciably below 1173 K [53]. A single phase of $\text{Mg}_{2.5}\text{VMoO}_8$ (**F**) was formed at 1173 K (Fig. 2). Temperatures of 1223 and 1323 K (which are below its peritectic melting point, 1423 K) were needed to incorporate the excess vanadium and molybdenum, respectively, into the $\text{Mg}_{2.5+x}\text{V}_{1+2x}\text{Mo}_{1-2x}\text{O}_8$ structure and form $\text{Mg}_{2.54}\text{V}_{1.08}\text{Mo}_{0.92}\text{O}_8$ (**E**) and $\text{Mg}_{2.46}\text{V}_{0.92}\text{Mo}_{1.08}\text{O}_8$ (**G**).

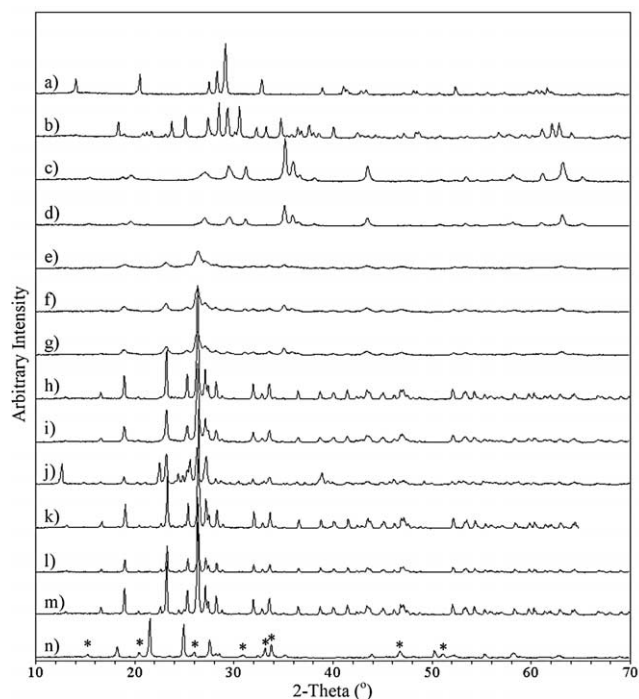


Fig. 1. Powder diffraction patterns for the sol–gel-prepared metal oxides calcined at 823 K: (a) MgV_2O_6 ; (b) $\text{Mg}_2\text{V}_2\text{O}_7$; (c) $\text{Mg}_3(\text{VO}_4)_2$; (d) $\text{Mg}_{2.98}(\text{V}_{0.98}\text{Mo}_{0.02}\text{O}_4)_2$; (e) 37.0% $\text{Mg}_3(\text{VO}_4)_2/\text{MgMoO}_4$; (f) 1:2 $\text{Mg}_3(\text{VO}_4)_2/\text{MgMoO}_4$; (g) 29.9% $\text{Mg}_3(\text{VO}_4)_2/\text{MgMoO}_4$; (h) $\text{Mg}_{0.992}\text{MoO}_{3.992}$; (i) $\text{Mg}_{1.015}\text{MoO}_{4.015}$; (j) MgMo_2O_7 ; (k) 2% V_2O_5 on MgMoO_4 ; (l) 1.86% V_2O_5 , 0.14% MoO_3 on MgMoO_4 ; (m) 1.72% V_2O_5 , 0.28% MoO_3 on MgMoO_4 ; (n) MoV_2O_8 , impurity V_2O_5 (*). Diffraction patterns were taken at room temperature in air.

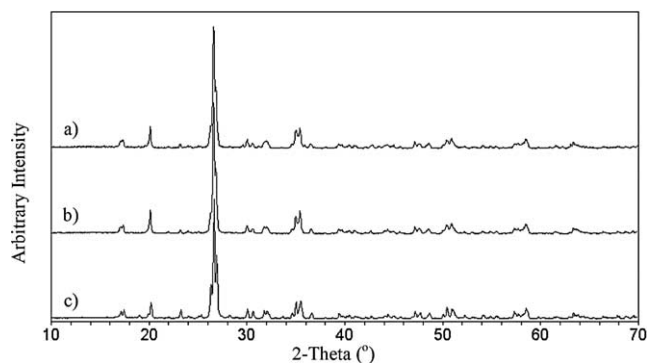


Fig. 2. Powder diffraction patterns of (a) $\text{Mg}_{2.54}\text{V}_{1.08}\text{Mo}_{0.92}\text{O}_8$; (b) $\text{Mg}_{2.5}\text{VMoO}_8$; (c) $\text{Mg}_{2.46}\text{V}_{0.92}\text{Mo}_{1.08}\text{O}_8$; calcined at 1173, 1223, and 1323 K, respectively. Diffraction patterns were taken at room temperature in air.

Combustion of the residual alkoxide moieties during the calcination of the $\text{Mg}_3(\text{VO}_4)_2$ precipitate was investigated with thermogravimetric analysis. Inspection of the TGA data showed a continuous weight loss of 25.2% upon increasing the temperature from room temperature to 723 K in flowing O_2 . However, no additional weight loss was observed upon increasing the temperature from 723 to 973 K. This implies that all of the organic compounds were combusted when the samples were calcined at 823 K for 12 h.

The physical properties of the metal oxides are summarized in Table 1. Surface areas increased as the Mg/V and Mg/Mo atomic ratios increased. This, in turn, is consistent with increasing melting points for the samples as the Mg/V and Mg/Mo atomic ratios increase. The low surface areas of the $\text{Mg}_{2.5+x}\text{V}_{1+2x}\text{Mo}_{1-2x}\text{O}_8$ samples (**E**, **F**, and **G**) are a result of the high calcination temperatures required to form single-phase samples.

Scanning electron micrographs (Fig. 3) of $\text{Mg}_2\text{V}_2\text{O}_7$ prepared by the solid-state technique, and $\text{Mg}_2\text{V}_2\text{O}_7$ (**B**) and $\text{Mg}_3(\text{VO}_4)_2$ (**C**) prepared by the sol–gel method, confirm the small (< 500 nm), uniform particle size of these metal oxides prepared by the sol–gel method at 823 K. The smaller size of the $\text{Mg}_2\text{V}_2\text{O}_7$ particles prepared by the sol–gel method compared with the sample synthesized by the solid-state technique is evident from the figures.

Raman spectra of select metal oxides are shown in Fig. 4. The spectra of $\text{Mg}_2\text{V}_2\text{O}_7$ (**B**), $\text{Mg}_3(\text{VO}_4)_2$ (**C**), and $\text{Mg}_{0.992}\text{MoO}_{3.992}$ (**I**) are consistent with previously reported spectra [54–56]. Minor shifts ($\leq 1\text{ cm}^{-1}$) in the peak positions between **C** and $\text{Mg}_{2.98}(\text{V}_{0.98}\text{Mo}_{0.02}\text{O}_4)_2$ (**D**) were detected but no additional peaks were found, confirming the absence of MgMoO_4 (996 cm^{-1}) and MoO_3 (826 cm^{-1}) [57]. Large backgrounds, due to fluorescence, were seen in the spectra of the 1:2 molar $\text{Mg}_3(\text{VO}_4)_2/\text{MgMoO}_4$ (**H**) and $\text{Mg}_{1.015}\text{MoO}_{4.015}$ (**J**). The background in the spectrum of **J** is so intense that the vibrational features barely can be discerned.

The source of fluorescence is difficult to attribute to a specific origin, because organic phases [58], trace transition metal impurities [58] (e.g., iron), and/or hydroxyl

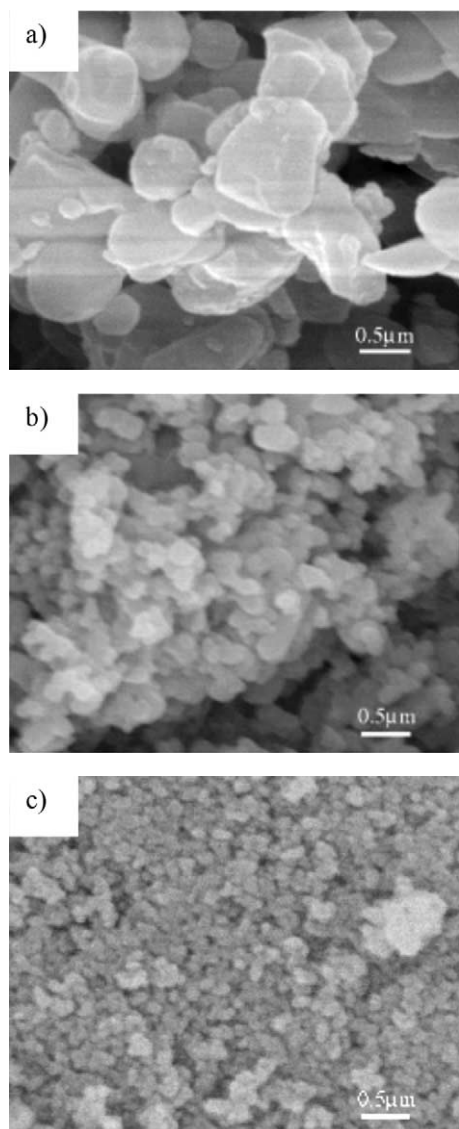


Fig. 3. SEM micrographs of (a) $\text{Mg}_2\text{V}_2\text{O}_7$ prepared by the solid-state technique calcined at 873 K; (b) $\text{Mg}_2\text{V}_2\text{O}_7$ prepared by a sol-gel method calcined at 823 K; (c) $\text{Mg}_3(\text{VO}_4)_2$ prepared by a sol-gel method calcined at 823 K.

groups [59] can cause fluorescence. It was established from the TGA experiments that an organic phase is not present and therefore cannot cause the fluorescence. Elemental analysis was used to analyze the compositions of the magnesium molybdate samples. Inductively coupled plasma-atomic emission spectrophotometry confirmed that the stoichiometries of the magnesium molybdates (**I** and **J**) were $\text{Mg}_{0.992}\text{MoO}_{3.992}$ and $\text{Mg}_{1.015}\text{MoO}_{4.015}$, respectively. Inductively coupled plasma-mass spectroscopy showed contamination of boron, silicon, phosphorous, and zinc on the parts per billion scale in the samples. The fluorescence was not attributed to these contaminants since they are found in both samples. These results suggests that the fluorescence originates from hydroxyl groups that would be present from the excess magnesium (as $\text{Mg}(\text{OH})_2$) in **J**.

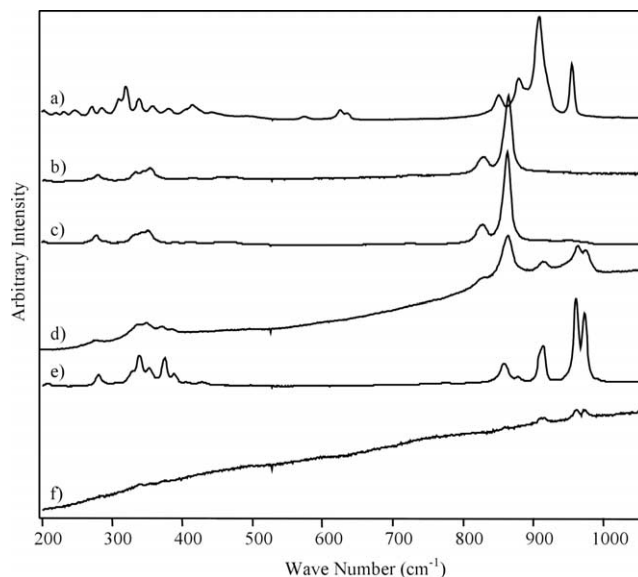


Fig. 4. Raman spectra of (a) $\text{Mg}_2\text{V}_2\text{O}_7$; (b) $\text{Mg}_3(\text{VO}_4)_2$; (c) $\text{Mg}_{2.98}(\text{V}_{0.98}\text{Mo}_{0.02}\text{O}_4)_2$; (d) 1:2 molar ratio of $\text{Mg}_3(\text{VO}_4)_2/\text{MgMoO}_4$; (e) $\text{Mg}_{0.992}\text{MoO}_{3.992}$; (f) $\text{Mg}_{1.015}\text{MoO}_{4.015}$.

3.2. Reaction studies

A summary of the gas-phase data from the propane ODH experiments is presented in Table 2. It is important to note that the reactant gas mixture is propane rich, and oxygen is the limiting reagent [60]. Therefore, the maximum obtainable conversion is 66.7% for an ODH reaction that is 100% selective with respect to the formation of propylene. No appreciable conversion was observed from the reactor or quartz chips at temperatures ≤ 808 K. The main products obtained during the catalytic testing were propylene, CO, and CO_2 ; occasionally, minor amounts of the liquid oxygenated products, acrolein, acrylic acid, acetic acid, propionic acid, acetone, and unknowns, were detected. When the oxygenated components are included in the calculations, the selectivities decrease by $< 1\%$, while the conversions increase by $< 2\%$. The carbon balance is within 95–105% for all of the reactions. Significant differences in the conversions and selectivities exist between the catalysts, so the results will be discussed in families of materials: the Mg–V–O, Mg–V–Mo–O, Mg–Mo–O, and the V–Mo–O-based catalysts.

The selectivity and conversion data of the vanadates (**A**, **B**, and **C**) are plotted in Fig. 5. MgV_2O_6 (**A**) exhibited higher selectivities and conversions than $\text{Mg}_2\text{V}_2\text{O}_7$ (**B**) and $\text{Mg}_3(\text{VO}_4)_2$ (**C**) at temperatures below 598 K, while **B** displayed the highest selectivities and conversions of **A**, **B**, and **C** at temperatures above 698 K. For example, **B** had a selectivity of 53.1% and conversion of 15.6% at 808 K. Catalyst **C** showed the lowest selectivities and conversions of **A**, **B**, and **C** at all temperatures. Additionally, a slight decrease in the conversion of **C** was observed after 24 h at 807 K from the initial conversion of 12.6 to 12.2%. This decrease is associated with coke formation detected with UV Raman spectroscopy. At temperatures above 698 K, the selectivities

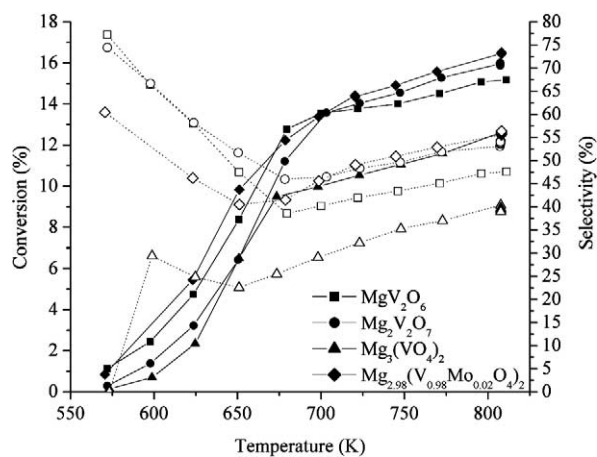


Fig. 5. Catalytic results for the ODH of propane with the Mg–V–O catalysts. Solid symbols correspond to the conversion, and hollow symbols correspond to selectivity. Test conditions: 30% C₃H₈, 10% O₂ (50 psig, 4000 GHSV, total flow = 133 sccm 14/30 mesh catalyst). Conversion and selectivity computed based on gas-phase components only.

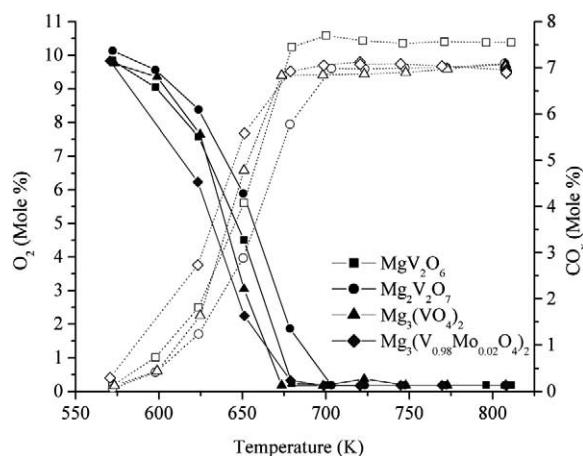


Fig. 6. Total O₂ and CO_x detected in the product stream of Mg–V–O catalysts during the ODH of propane. Solid symbols correspond to the O₂, and hollow symbols correspond to CO_x. Test conditions: 30% C₃H₈, 10% O₂, and 60% N₂ (50 psig, 4000 GHSV, total flow = 133 sccm 14/30 mesh catalyst). Conversion and selectivity computed based on gas-phase components only.

and conversions of the catalysts decreased as follows: **B** > **A** > **C**. These results parallel the electrical conductivity and band-gap energy data reported by Volta and co-workers and described in the Introduction [27].

The initial selectivities decreased with increasing conversion, but, interestingly, at temperatures above 673 K the selectivities began to increase with increasing conversions. This phenomenon is related to the complete depletion of O₂ in the reactant stream (Fig. 6). Upon depletion of O₂ from the reactant stream, the increase in propane conversion observed as the temperature increases occurs with an additional consumption of the lattice oxygen from the catalyst, thereby reducing the catalyst, as observed in the visible and UV Raman spectroscopy measurements of Mg₃(VO₄)₂ (**C**) and Mg_{0.992}MoO_{3.992} (**I**). Note, however, that the selective for-

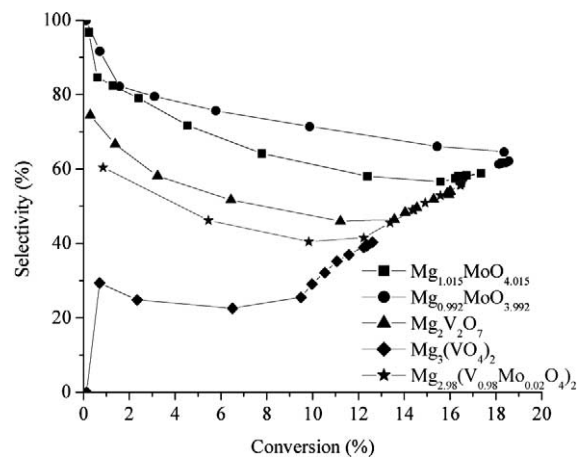


Fig. 7. Conversion versus selectivity. Test conditions: 30% C₃H₈, 10% O₂ (50 psig, 4000 GHSV, total flow = 133 sccm 14/30 mesh catalyst). Data computed based on gas-phase components only.

mation of propylene after oxygen depletion is also accompanied by an unvarying production of CO_x. In general, the amount of CO produced increased while the CO₂ decreased as the temperature increased and the reaction proceeded, and this shift from CO₂ to CO provides a quantitative marker, based on the oxygen mass balance, for the increase in selective ODH. The calculated increase in the propylene selectivity and conversion for Mg₂V₂O₇ (**B**) that results from the shift of CO₂ to CO between 703 and 807 K is 5.2% (46.4 to 51.6%) and 1.6% (13.6 to 15.2%), respectively. Thus, when depletion of O₂ in the reactant stream occurs and as the temperature increases, a more efficient utilization of oxygen is realized leading to an increase in selectivity. In addition, while the analysis of hydrogen was not performed, the dehydrogenation reaction is also likely to contribute to the selective conversion of propylene. The observation of coke formation, which typically accompanies catalytic dehydrogenation, was detected by UV Raman spectroscopy measurements on the Mg₃(VO₄)₂ (**C**) catalyst following reaction at 723 and 798 K. Based on the good agreement between the observed selectivity of propylene 53.1% (see Fig. 5) versus the percentage calculated or expected from the shift of CO₂ to CO (51.6%), the dehydrogenation reaction appears to make a minor contribution. Consistent with these observations, the data acquired after oxygen depletion lie on a single curve when conversion versus selectivity is plotted (Fig. 7). This suggests that the surface structure(s), and perhaps the active site(s), of the reduced magnesium vanadates (**A**, **B**, and **C**) and molybdates (**I** and **J**) are similar, although there could be other possible explanations.

A significant improvement in the conversion and selectivity of Mg₃(VO₄)₂ (**C**) was observed with the substitution of molybdenum into the structure. Catalyst **C** reached 10% conversion at 698 K with a 29.1% selectivity for propylene. In contrast, Mg_{2.98}(V_{0.98}Mo_{0.02}O₄)₂ (**D**) reached 10% conversion at 652 K with a selectivity of 40.6%. Additionally, **D** exhibited a higher conversion (16.5%) and selectivity (55.6%) than **A**, **B**, and **C** at 808 K. A small increase in

the liquid oxygenated products (0.37% vs 0.11%), primarily acrolein, was observed with the molybdenum substitution.

The increase in conversion and selectivity seen with molybdenum substitution is associated with Mg cation vacancies formed from the substitution of Mo^{6+} for V^{5+} . The data suggest that these cation vacancies allow for a more facile diffusion of the lattice oxygen to the surface of the catalyst. Furthermore, the cation vacancy is electron rich, rendering the oxide anions more basic. The more basic oxide anion can more easily abstract a hydrogen atom from the adsorbed propane. Similar increases in conversion and selectivity associated with cation vacancies have been seen with other oxidation catalysts [61–66]. Sleight and Linn attribute the increase in selectivity and activity to the more basic nature of the oxide anions, promoting allyl formation [61]. Tsunoda et al. [63] and Fan et al. [62] suggest that the increase in activity is due to the more facile diffusion of the oxide anions through the bulk structure. Li and co-workers propose that the cation vacancies allow for the formation of $\text{Mo}=\text{O}$ and distorts the $\text{Mo}(\text{V})\text{O}_4$ tetrahedron creating a stronger $\text{Bi}-\text{O}-\text{V}$ bond [64]. They suggest the enhanced selectivity results from the $\text{Mo}=\text{O}$ double bond, and that the increased conversion is due to a synergistic effect between the $\text{Mo}=\text{O}$ and the $\text{Bi}-\text{O}-\text{V}$ bonds [64].

The magnesium vanadium molybdates (**E**, **F**, and **G**) showed the lowest conversions of all the catalysts tested (Fig. 8). The $\text{Mg}_{2.5}\text{VMoO}_8$ catalyst (**F**) reached a maximum conversion of only 5.4% with a selectivity of 40.2%. Again, the conversions and selectivities of the catalysts increased with increasing molybdenum substitution. The $\text{Mg}_{2.54}\text{V}_{1.08}\text{Mo}_{0.92}\text{O}_8$ sample (**E**) had a conversion of 4.6% and selectivity of 38.4% at 808 K, but an increase of the molybdenum content to $\text{Mg}_{2.46}\text{V}_{0.92}\text{Mo}_{1.08}\text{O}_8$ (**G**) improved the conversion (10.4%) and selectivity (46.0%). Catalyst **G**

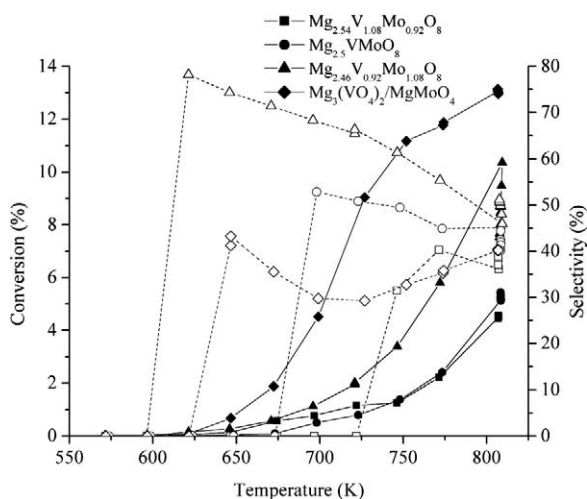


Fig. 8. Catalytic results for the ODH of propane with the Mg–V–Mo–O catalysts. Solid symbols correspond to the conversion, and hollow symbols correspond to selectivity. Test conditions: 30% C_3H_8 , 10% O_2 (50 psig, 4000 GHSV, total flow = 133 sccm 14/30 mesh catalyst). Conversion and selectivity computed based on gas-phase components only.

had a comparable conversion and better selectivity than **C** at 808 K, which is similar to the results seen with the ODH of *n*-butane [37]. In contrast to the previous results seen with **C** and **D**, smaller amounts of oxygenated products formed with increasing molybdenum concentration (0.39 and 0.95% for **G** and **E**, respectively). An increase in selectivity with increasing conversion was not observed because the oxygen was not depleted in the reactant stream as a result of the low conversions.

Magnesium molybdates (**I**, **J**, and **K**) exhibited lower conversions than the vanadates (**A**, **B**, and **C**) at temperatures below 723 K. For example, the vanadates reached 5% conversion at temperatures near 630 K, whereas the molybdates reached the 5% conversion at ~ 700 K. The rate of propane conversion over the molybdate catalysts increased quickly, such that at higher temperatures the molybdates exhibited higher conversions than the vanadates. At identical conversions, the molybdates were more selective than the vanadates. Weaker metal–oxygen bonds have been shown to increase the activity, but decrease the selectivity of the reaction [29,67,68]. Chen et al. show that a decrease in the UV–visible absorption-edge energy of metal oxide catalysts correlates to an increase in the propane ODH turnover rate [69]. They state that the energy required to transfer electrons from the oxygen to the metal is an indication of the C–H bond activation energy and that as the metal–oxygen bond becomes more difficult to break, the turnover rate of propane ODH decreases [69].

The catalytic behavior of the magnesium molybdates (**I**, **J**, and **K**) is shown in Fig. 9. The $\text{Mg}_{0.992}\text{MoO}_{3.992}$ (**I**) exhibited the highest conversion (18.6%) and selectivity (61.8%) and produced the most oxygenated products (3.08 with 0.96% acetic acid, 0.82% acrylic acid, 0.32% acrolein, and other oxygenates) of all the catalysts tested. The $\text{Mg}_{1.015}\text{MoO}_{4.015}$ (**J**) had a conversion curve similar to **I**, but was less active at higher temperatures. The selec-

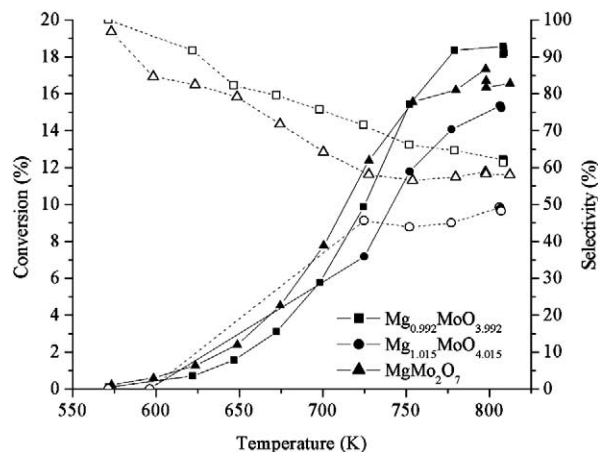


Fig. 9. Catalytic results for the ODH of propane with the Mg–Mo–O catalysts. Solid symbols correspond to the conversion, and hollow symbols correspond to selectivity. Test conditions: 30% C_3H_8 , 10% O_2 (50 psig, 4000 GHSV, total flow = 133 sccm 14/30 mesh catalyst). Conversion and selectivity computed based on gas-phase components only.

tivity of **J** was lower than **I** at all temperatures, but fewer oxygenates formed (0.36%) with **J**. These results agree with those seen previously in other reports; that is, MgMoO_4 with a slight excess of MoO_3 shows a higher activity and selectivity than samples with an excess of MgO [13,34,70]. In addition, complete oxygen depletion from the feed stream was observed only at 808 K for **I** and **J**; thus, an increase of selectivity with conversion was not observed. The MgMo_2O_7 (**K**) exhibited a lower selectivity than **I** at all temperatures. Catalyst **K** exhibited higher selectivities and conversions than **J** and higher conversions than sample **I** at lower temperatures (< 748 K).

The conversions and selectivities of the supported $\text{V}_{2-2x}\text{Mo}_{2x}\text{O}_{5+x}$ catalysts (**L**, **M**, and **N**) are similar to **I** (Fig. 10). For example, selectivities of 59.3, 60.5, and 60.4% and conversions of 16.8, 18.2, and 17.8% were observed for **L**, **M**, and **N**, respectively, at 808 K. However, the selectivities of **L**, **M**, and **N** begin to increase at ~ 725 K, because of oxygen depletion from the reactant stream. These data imply that the surfaces of **L**, **M**, and **N** were not as selective as **I** for the formation of propylene.

Molybdenum divanadium oxide, MoV_2O_8 (**O**), exhibited the highest conversion (1.8%) at 573 K of all catalysts tested, but the conversion did not increase as fast as the other catalysts. **O** displayed the lowest selectivity (15.6%) at 698 K before increasing to 35.5%, the lowest selectivity observed at 808 K. These results can be explained by the presence of V_2O_5 . Kung and co-workers report that V_2O_5 exhibits high conversions for alkane ODH but low selectivities for alkene formation [7,26].

The 1:2 molar mixture of $\text{Mg}_3(\text{VO}_4)_2/\text{MgMoO}_4$ (**H**) displayed a higher conversion than the magnesium vanadium molybdates (**E**, **F**, and **G**), but at equivalent conversions the selectivity of **H** was lower. The selectivity and conversion of **H** were similar to those of catalyst **C** but were lower

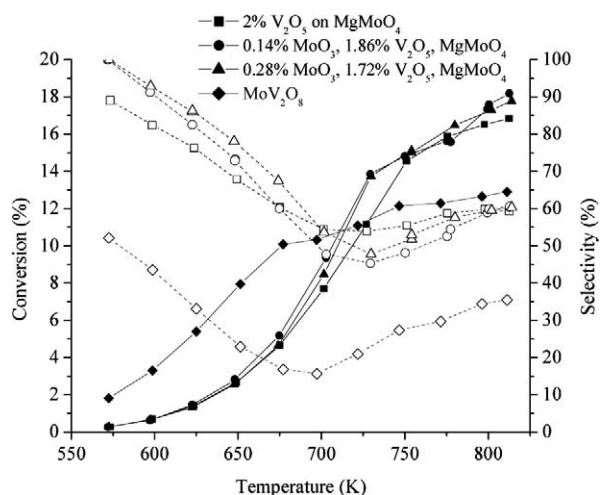


Fig. 10. Catalytic results for the ODH of propane with the Mo–V–O catalysts. Solid symbols correspond to the conversion, and hollow symbols correspond to selectivity. Test conditions: 30% C_3H_8 , 10% O_2 (50 psig, 4000 GHSV, total flow = 133 scfm 14/30 mesh catalyst). Conversion and selectivity computed based on gas-phase components only.

than both **I** and **J**. A slight increase (0.04%) in the amount of liquid oxygenates produced by mixture **H** was observed, compared to **D**.

As shown above, supported vanadium oxide catalysts (**L**, **M**, and **N**) have conversions and selectivities similar to those of the single-phase catalysts (**J**). The surfaces of supported catalysts can be described as two-dimensional structures of monomers or oligomers that are bonded to a metal oxide. However, Wachs and co-workers report data that indicate the bulk Fe–V and Al–V vanadates have specific activities which are nearly an order of magnitude greater than the respective monolayer vanadium oxide-supported catalyst, while that of bulk Ni–V is approximately two orders of magnitude greater than the monolayer vanadium oxide-supported catalyst [71].

The results presented here show the importance of the bulk catalyst structure on the catalytic selectivity and conversion. The bulk structure allows the catalysts to continuously undergo reduction and reoxidation cycles during reaction conditions, at steady state. However, the ODH reactions occur at the catalyst surface. Therefore, the catalyst surface structure needs to be resolved to allow for a fundamental understanding of the reaction pathway that occurs at the catalyst surface.

3.3. Raman studies

The visible Raman spectrum of $\text{Mg}_3(\text{VO}_4)_2$ (**C**) at room temperature matches previously reported spectra [72,73] (Fig. 11). The UV Raman spectrum is in good agreement with the visible Raman spectrum, but an additional peak is observed in the UV Raman spectrum at 650 cm^{-1} (Fig. 12). This additional peak is assigned to the V–O–Mg stretching mode because the V–O–In of InVO_4 [74], the V–O–Fe of FeVO_4 [74], and the V–O–V of $\text{Mg}_2\text{V}_2\text{O}_7$ [73] and rare earth orthovanadates [75] are centered near 650 cm^{-1} . The

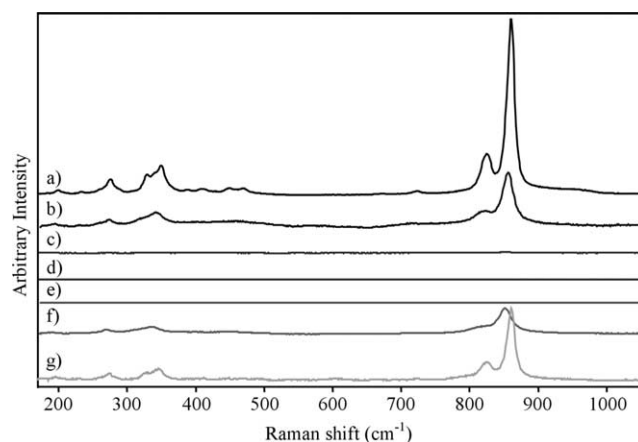


Fig. 11. Visible Raman spectra of $\text{Mg}_3(\text{VO}_4)_2$. The spectra were taken under in situ conditions (30% C_3H_8 , 10% O_2 , and 60% N_2 flowing at 50 sccm) at: (a) 303 K; (b) 623 K; (c) 673 K; (d) 723 K; (e) 798 K. Spectrum (f) was taken after (e) under a flow of air at 798 K. Spectrum (g) was taken of fresh catalyst under a flow of He at 798 K.

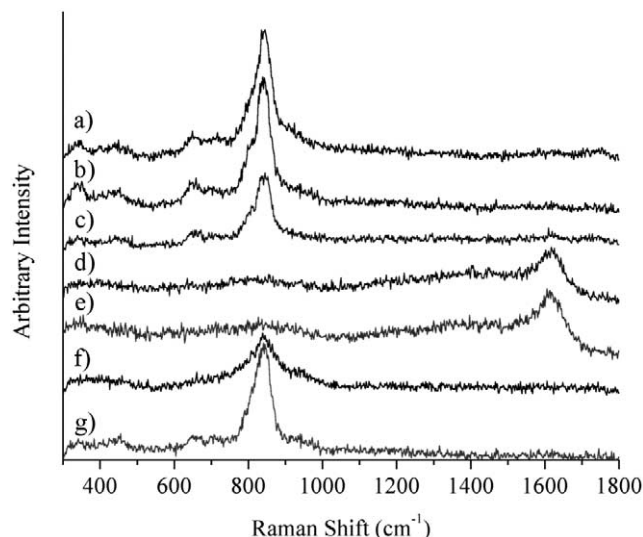


Fig. 12. UV Raman spectra of $\text{Mg}_3(\text{VO}_4)_2$. The spectra were taken after the catalysts were exposed to reaction conditions (30% C_3H_8 , 10% O_2 , and 60% N_2 flowing at 50 sccm) for 1 h at: (a) 298 K; (b) 623 K; (c) 673 K; (d) 723 K; (e) 798 K. Spectrum (f) was taken after (e) exposed to a 5 sccm flow of O_2 at 798 K. Spectrum (g) was taken of fresh catalyst exposed to a 1-h flow of He at 798 K. All spectra were taken for 1 h at room temperature under flowing N_2 .

Table 3

In situ visible Raman peak positions (cm^{-1}) for $\text{Mg}_3(\text{VO}_4)_2$					
30 °C	350 °C	400 °C	450 °C ^a	525 °C ^a	525 °C air
860	854	853			850
825	821				SH ^b
722					
469					
448					
409					
387					
349	339	336			335
329	SH				SH
275	271				268
233	228				226
198	192				188

^a Spectrum recorded but no observable features.

^b SH indicates shoulder.

peak is evident in the UV Raman spectrum because the exciting photon energy (5.1 eV) is near the VO_4^{3-} band gap (~ 5 eV) [76–78], thus enhancing the intensity of the stretching mode [79,80]. The broad peaks at ~ 1610 cm^{-1} in Fig. 12(d and e), are associated with coke formation from propane dehydrogenation at the high temperatures [81]. The peak positions shifted to lower frequencies as the in situ temperature increases (Table 3) [82]. The gradual disappearance of the Raman bands associated with the symmetric stretch (ν_1 , 860 cm^{-1}), asymmetric stretch (ν_3 , 825 cm^{-1}), asymmetric bend (ν_4 , 722 cm^{-1}), and symmetric bend (ν_2 , 349 cm^{-1}) of the VO_4^{3-} [82] indicates the reduction of the sample. The catalyst appeared black when it was visually inspected in the UV Raman cell after the ODH reaction at 723 K. The Raman bands did not disappear upon heating

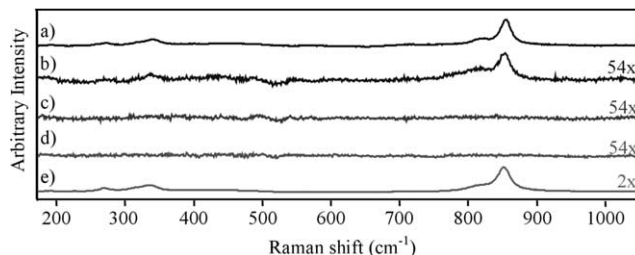


Fig. 13. Magnification of the visible Raman spectra of $\text{Mg}_3(\text{VO}_4)_2$. The spectra were taken under in situ conditions (30% C_3H_8 , 10% O_2 , and 60% N_2 flowing at 50 sccm) at: (a) 623 K; (b) 673 K; (c) 723 K; (d) 798 K. Spectrum (e) was taken at 798 K under a flow of air.

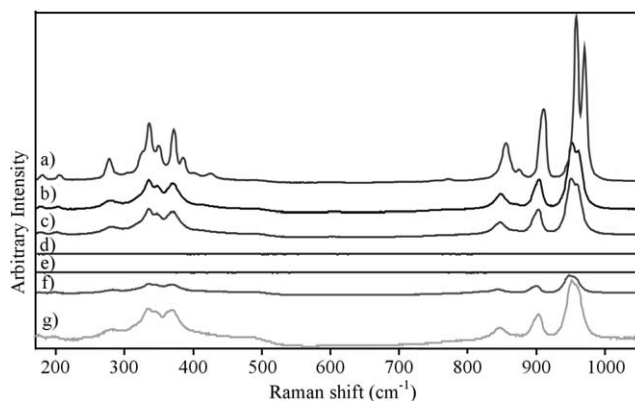


Fig. 14. Visible Raman spectra of $\text{Mg}_{0.992}\text{MoO}_{3.992}$. The spectra were taken under in situ conditions (30% C_3H_8 , 10% O_2 , and 60% N_2 flowing at 50 sccm) at: (a) 303 K; (b) 623 K; (c) 673 K; (d) 723 K; (e) 798 K. Spectrum (f) was taken after (e) under a flow of air at 798 K. Spectrum (g) was taken of fresh catalyst under a flow of He at 798 K.

fresh C at 798 K in flowing helium; therefore, the reduction of the catalyst during the replicated reaction conditions cannot be attributed to thermal reduction (Figs. 11(g) and 12(g)). Upon reoxidation, the catalyst turned white in color and the Raman peaks reappeared.

Interestingly, the temperature (673 K) at which the visible Raman bands disappeared corresponds to the temperature where oxygen was not detected in the reaction stream, for the first time, during the catalytic testing. Magnification of the visible Raman spectrum taken at 673 K reveals a small peak at ~ 853 cm^{-1} (Fig. 13), indicating that the catalyst is not fully reduced. The catalyst is reduced further at higher temperature. Indeed, no Raman features of the VO_4^{3-} tetrahedra are observed upon magnification of the spectra taken at 723 and 798 K, excited by visible and ultraviolet light.

The visible and UV Raman spectra of $\text{Mg}_{0.992}\text{MoO}_{3.992}$ (I) at room temperature match the previously reported spectrum [83] (Figs. 14 and 15). The lack of agreement between the peak positions and those reported for the hydrated MgMoO_4 indicates that water is not coordinated to the sample [84]. In the UV Raman spectrum, the peaks at ~ 979 and 950 cm^{-1} are not resolved. Most of the peak positions shift to lower frequencies as the temperature increases for the in situ experiments (Table 4). The disappearance of the Ra-

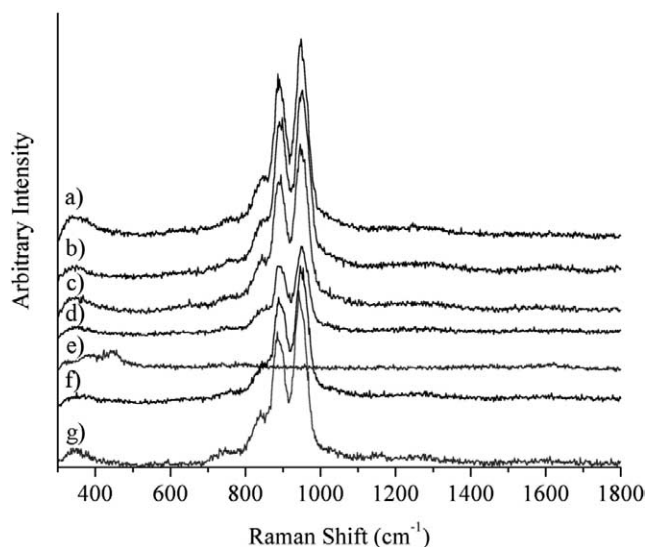


Fig. 15. UV Raman spectra of $\text{Mg}_{0.992}\text{MoO}_{3.992}$. The spectra were taken after the catalysts were exposed to reaction conditions (30% C_3H_8 , 10% O_2 , and 60% N_2 flowing at 50 sccm) for 1 h at: (a) 298 K; (b) 623 K; (c) 673 K; (d) 723 K; (e) 798 K. Spectrum (f) was taken after (e) exposed to a 5 sccm flow of O_2 at 798 K. Spectrum (g) was taken of fresh catalyst exposed to a 1-h flow of He at 798 K. All spectra were taken for 1 h at room temperature under flowing N_2 .

Table 4
In situ visible Raman peak positions (cm^{-1}) for $\text{Mg}_{0.992}\text{MoO}_{3.992}$

30 °C	350 °C	400 °C	450 °C	525 °C	525 °C air/He
970	961	SH			SH ^a
958	952	951	950	950	947
910	904	902	900		900
874					
855	848	848			843
424					
385					
371	370	370			369
349	347	347			
335	335	335	335	335	335
277	280	280			282
204	202	202			198
180	177	177			176

^a SH indicates shoulder.

man peaks corresponding to the symmetric stretch (ν_1 , 900 and 958 cm^{-1}), asymmetric stretch (ν_3 , 910 and 874 cm^{-1}), asymmetric bend, and symmetric bend of the MoO_4^{2-} [83] indicates the reduction of the sample. The catalyst appeared gray when it was visually inspected in the cells after the reaction at 798 K. The reduction of **I** during in situ conditions cannot be attributed to thermal reduction as the vibrational bands did not disappear upon heating fresh catalyst at 798 K in flowing helium (Figs. 14(g) and 15(g)). Interestingly, a new band appears at $\sim 445\text{ cm}^{-1}$ in the UV Raman spectrum after the reaction at 798 K. The peak position is attributed to the stretching mode of three-coordinate oxygen and not bridging oxygen, because no additional peaks at higher Raman shifts were observed. This peak is similar to the three-coordinate vibration seen with high-resolution

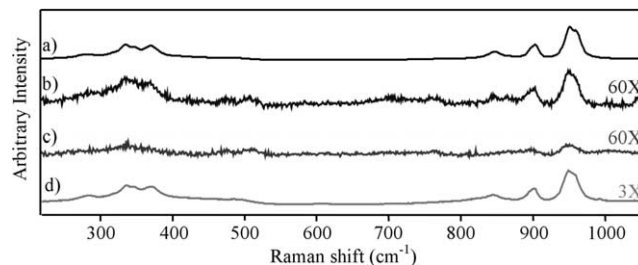


Fig. 16. Magnification of the visible Raman spectra of $\text{Mg}_{0.992}\text{MoO}_{3.992}$. The spectra were taken under in situ conditions (30% C_3H_8 , 10% O_2 , and 60% N_2 flowing at 50 sccm) at: (a) 673 K; (b) 723 K; (c) 798 K. Spectrum (d) was taken at 798 K under a flow of air.

electron energy loss spectroscopy (HREELS) on an oxygen-modified Mo (100) surface [85]. The peak shift to a lower wavenumber than that observed in the HREELS experiment is due to the weaker bond strength from the higher Mo oxidation state of the reduced **I**. Upon reoxidation, the catalyst turned pale gray in color and the Raman peaks reappeared. The Raman bands associated with the three-coordinate oxygen of the reduced catalyst disappeared.

Again, a correlation exists between the peak intensity and the catalyst reduction. Bands from the visible excitation taken at 723 and 798 K seem to disappear. However, small peaks are apparent upon magnification of the spectra (Fig. 16). No Raman features are observed for the spectrum taken at 798 K, even after magnification. The difference in the UV and visible Raman features is due to the “skin depth” penetration, the minimum depth of material probed which is determined by the absorptivity of the sample and given by $\lambda/(4\pi k)$, where λ is the laser wavelength and k is the imaginary part of the complex refractive index of the sample [86]. To the best of the author’s knowledge there is no direct information on the k value of the $\text{Mg}_3(\text{VO}_4)_2$ and MgMoO_4 , so the skin depth is estimated using similar solids as models [87]. At 244 nm (514.5 nm), the skin depth of KNbO_3 is calculated to be 12.1 nm, that of BaTiO_3 is 14.9 nm (28.4 nm), and that of SrTiO_3 is 15.1 nm (27.6 nm). The skin depths of the materials at 244 nm are approximately half the skin depths at 514.5 nm. Therefore, the catalyst surface contributes more to the UV Raman signal than the visible Raman signal. The Raman data imply that the surface of the catalyst is reduced but the bulk is still oxidized. This explanation is consistent with the reaction data.

The Raman data combined with the reaction data demonstrate that the ODH of propane is consistent with the Mars–van Krevelen reaction mechanism. Although the peak intensities decrease during the reaction with propane, peaks are observed in the in situ Raman spectra until the gas-phase O_2 in the reaction stream had been consumed in the reaction. At this point, further reaction reduces the catalyst and the peaks associated with the $\text{VO}_4^{3-}/\text{MoO}_4^{2-}$ cannot be detected. The reactor data show that the O_2 (g) had completely reacted by 673 K with catalyst **C**. Propane further reacted with lattice oxygen resulting in the reduction of the catalyst. However, gas-phase oxygen was still present during the re-

action at 798 K with catalyst **I**, so the catalyst was never fully reduced.

4. Conclusions

In order to compare the reactivity of magnesium vanadates and magnesium molybdates in the same ODH study, a series of metal oxides from the $\text{MgO}-\text{V}_2\text{O}_5-\text{MoO}_3$ ternary phase diagram have been prepared. These samples were examined for the oxidative dehydrogenation of propane. From the catalytic data presented above, the magnesium vanadate selectivities and conversions decrease as follows $\text{Mg}_2\text{V}_2\text{O}_7 > \text{MgV}_2\text{O}_6 > \text{Mg}_3(\text{VO}_4)_2$ at temperatures greater than 723 K. The vanadates exhibited higher conversions than the molybdates at identical temperatures below 723 K; however, the molybdates exhibited a lower selectivity at identical conversions. $\text{Mg}_{0.992}\text{MoO}_{3.992}$ exhibited the highest selectivity and conversion (at 808 K) of the catalysts tested. Compared with $\text{Mg}_{0.992}\text{MoO}_{3.992}$, the recorded yields from the samples comprised of $\text{V}_{2-2x}\text{Mo}_{2x}\text{O}_{5+x}$ supported on MgMoO_4 are nearly the same (at 808 K). However, complete oxygen depletion occurred at ~ 723 K for the supported $\text{V}_{2-2x}\text{Mo}_{2x}\text{O}_{5+x}$ catalysts but not until 808 K for $\text{Mg}_{0.992}\text{MoO}_{3.992}$, thus implying that the surfaces of the supported catalysts are less selective than $\text{Mg}_{0.992}\text{MoO}_{3.992}$.

In general, it was observed that the selectivities increased with increasing conversions at temperatures above 673 K. This phenomenon is related to the complete depletion of O_2 in the reactant stream. The increase of selectivity with increasing conversion largely results from the more efficient use of the oxidant (O_2) while propane reacts on these surfaces. In addition, the data suggest that the surface structure(s), and perhaps the active site(s), of the reduced magnesium vanadates (**A**, **B**, and **C**) and molybdates (**I** and **J**) are similar.

Additionally, the effect of molybdenum substitution into various structures was examined. A significant improvement in the selectivity and conversion was observed with the substitution of molybdenum into various structures. The increase in selectivity and conversion seen with molybdenum substitution is associated with Mg cation vacancies formed from the substitution of Mo^{6+} for V^{5+} . The cation vacancies result in a more basic oxide anion and the data suggest that the vacancies allow a more facile diffusion of the lattice oxygen to the surface of the catalyst.

The visible and UV Raman spectra of $\text{Mg}_3(\text{VO}_4)_2$ and $\text{Mg}_{0.992}\text{MoO}_{3.992}$ exposed to replicated reaction conditions exhibit some different spectral features, including the Raman spectra of $\text{Mg}_3(\text{VO}_4)_2$ at 673 and 723 K, allowing for more surface-specific information. The difference in the “skin depth” penetration results in the UV Raman spectroscopy being a more surface-sensitive probe than visible Raman spectroscopy. The Raman bands shift to lower frequencies as the temperature is increased during the in situ conditions. The gradual disappearance of the Raman peaks during the

experiments correlates with the reaction of propane and the lattice oxygen, reducing the catalyst. These data combined with the reactor data demonstrate that the oxidative dehydrogenation of propane occurs by the Mars–van Krevelen reaction mechanism.

A new band centered at 445 cm^{-1} is observed in the UV Raman spectrum for the reduced $\text{Mg}_{0.992}\text{MoO}_{3.992}$ and is attributed to the stretching mode of three-coordinate oxygen. This new feature can give insight into the structural changes the catalyst undergoes during the ODH reaction. Furthermore, the appearance of new features helps to focus our attention to surfaces that may exhibit reconstruction upon reduction.

These results illustrate the importance of determining the reaction pathway in atomic detail. A fundamental understanding of the molecule-transforming chemistry that occurs on solid surfaces and the reaction mechanism in the bulk of the catalysts will allow for the development of catalysts with increased selectivities and conversions and improved yields.

Acknowledgments

The authors thank Erl Thorsteinson for setting up this collaboration and his helpful discussions and Richard Chaffin for the Krypton BET surface area measurements. The authors gratefully acknowledge support by the National Science Foundation and the Department of Energy under the Environmental Molecular Science Institutes program (Grant 9810378) at the Northwestern University Institute for Environmental Catalysis and made use of the Central Facilities supported by the MRSEC program of the National Science Foundation (Grant DMR-0076097) at the Materials Research Center of Northwestern University. B. Bardin acknowledges The Dow Chemical Company for support of this work.

References

- [1] F. Cavani, F. Trifiro, *Catal. Today* 24 (1995) 307–313.
- [2] E.A. Mamedov, V. Cortes Corberan, *Appl. Catal. A* 127 (1995) 1–40.
- [3] M.M. Bettahar, G. Costentin, L. Savary, J.C. Lavalley, *Appl. Catal. A* 145 (1996) 1–48.
- [4] S. Albonetti, F. Cavani, F. Trifiro, *Catal. Rev.—Sci. Eng.* 38 (1996) 413–438.
- [5] T. Blasco, J.M. Lopez Nieto, *Appl. Catal. A* 157 (1997) 117–142.
- [6] H.H. Kung, M.C. Kung, *Appl. Catal. A* 157 (1997) 105–116.
- [7] M.A. Chaar, D. Patel, H.H. Kung, *J. Catal.* 109 (1988) 463–467.
- [8] D.S.H. Sam, V. Soenen, J.C. Volta, *J. Catal.* 123 (1990) 417–435.
- [9] A. Corma, J.M. Lopez Nieto, N. Paredes, *J. Catal.* 144 (1993) 425–438.
- [10] A. Corma, J.M.L. Nieto, N. Paredes, A. Dejoz, I. Vazquez, *Stud. Surf. Sci. Catal.* 82 (1994) 113–123.
- [11] X. Gao, P. Ruiz, Q. Xin, X. Guo, B. Delmon, *J. Catal.* 148 (1994) 56–67.
- [12] Z. Fang, W. Weng, H. Wan, K. Tsai, *Fenzi Cuihua* 9 (1995) 401–410.
- [13] C. Mazzocchia, C. Aboumradi, C. Diagne, E. Tempesti, J.M. Herrmann, G. Thomas, *Catal. Lett.* 10 (1991) 181–191.

- [14] Y.S. Yoon, W. Ueda, Y. Moro-oka, *Catal. Lett.* 35 (1995) 57–64.
- [15] M.C. Abello, M.F. Gomez, L.E. Cadus, *Ind. Eng. Chem. Res.* 35 (1996) 2137–2143.
- [16] W. Ueda, K.H. Lee, Y.S. Yoon, Y. Moro-oka, *Catal. Today* 44 (1998) 199–203.
- [17] J.E. Miller, N.B. Jackson, L. Evans, A.G. Sault, M.M. Gonzales, *Catal. Lett.* 58 (1999) 147–152.
- [18] V. Soenen, J.M. Herrmann, J.C. Volta, *J. Catal.* 159 (1996) 410–417.
- [19] D. Creaser, B. Andersson, *Appl. Catal. A* 141 (1996) 131–152.
- [20] K. Chen, A. Khodakov, J. Yang, A.T. Bell, E. Iglesia, *J. Catal.* 186 (1999) 325–333.
- [21] L. Late, E.A. Blekkan, *J. Nat. Gas Chem.* 11 (2002) 33–42.
- [22] M. Sautel, G. Thomas, A. Kaddouri, C. Mazzocchia, R. Anouchinsky, *Appl. Catal. A* 155 (1997) 217–228.
- [23] D.L. Stern, R.K. Grasselli, *J. Catal.* 167 (1997) 560–569.
- [24] K. Chen, E. Iglesia, A.T. Bell, *J. Phys. Chem. B* 105 (2001) 646–653.
- [25] P. Mars, D.W. van Krevelen, *Chem. Eng. Sci.* 3 (1954) 41–59.
- [26] M.A. Chaar, D. Patel, M.C. Kung, H.H. Kung, *J. Catal.* 105 (1987) 483–498.
- [27] A. Guerrero-Ruiz, I. Rodriguez-Ramos, J.L.G. Fierro, V. Soenen, J.M. Herrmann, J.C. Volta, *Stud. Surf. Sci. Catal.* 72 (1992) 203–212.
- [28] M.C. Kung, H.H. Kung, *J. Catal.* 134 (1992) 668–677.
- [29] O.S. Owen, H.H. Kung, *J. Mol. Catal.* 79 (1993) 265–284.
- [30] N. Krishnamachari, C. Calvo, *Can. J. Chem.* 49 (1971) 1629–1637.
- [31] R. Gopal, C. Calvo, *Acta Crystallogr., Sect. B* 30 (1974) 2491–2493.
- [32] A. Corma, J.M. Lopez Nieto, N. Paredes, *Appl. Catal. A* 104 (1993) 161–174.
- [33] N. Fujikawa, Y.S. Yoon, W. Ueda, Y. Moro-oka, *Trans. Mater. Res. Soc. Jpn. A* 15 (1994) 79–82.
- [34] L.E. Cadus, M.C. Abello, M.F. Gomez, J.B. Rivarola, *Ind. Eng. Chem. Res.* 35 (1996) 14–18.
- [35] L.E. Cadus, M.F. Gomez, M.C. Abello, *Catal. Lett.* 43 (1997) 229–233.
- [36] K.H. Lee, Y.S. Yoon, W. Ueda, Y. Moro-oka, *Catal. Lett.* 46 (1997) 267–271.
- [37] W.D. Harding, H.H. Kung, V.L. Kozhevnikov, K.R. Poepplmeier, *J. Catal.* 144 (1993) 597–610.
- [38] X. Wang, C.L. Stern, K.R. Poepplmeier, *J. Alloys Compd.* 243 (1996) 51–58.
- [39] V.G. Zubkov, I.A. Leonidov, K.R. Poepplmeier, V.L. Kozhevnikov, *J. Solid State Chem.* 111 (1994) 197–201.
- [40] R.A. Overbeek, M. Versluijs-Helder, P.A. Warringa, E.J. Bosma, J.W. Geus, *Stud. Surf. Sci. Catal.* 82 (1994) 183–193.
- [41] G. Mestl, T.K.K. Srinivasan, H. Knoezinger, *Langmuir* 11 (1995) 3795–3804.
- [42] C. Li, P.C. Stair, *Catal. Lett.* 36 (1996) 119–123.
- [43] Z.-X. Gao, H.-S. Kim, Q. Sun, P.C. Stair, W.M.H. Sachtler, *J. Phys. Chem. B* 105 (2001) 6186–6190.
- [44] M.A. Banares, I.E. Wachs, *J. Raman Spectrosc.* 33 (2002) 359–380.
- [45] Y. Chen, I.E. Wachs, *J. Catal.* 217 (2003) 468–477.
- [46] G.T. Went, L.J. Leu, R.R. Rosin, A.T. Bell, *J. Catal.* 134 (1992) 492–505.
- [47] B.M. Weckhuysen, I.E. Wachs, *J. Phys. Chem.* 100 (1996) 14437–14442.
- [48] C.-B. Wang, Y. Cai, I.E. Wachs, *Langmuir* 15 (1999) 1223–1235.
- [49] Y.T. Chua, P.C. Stair, *J. Catal.* 196 (2000) 66–72.
- [50] G.E. Selyutin, N.G. Maksimov, G.A. Zenkovets, D.V. Tarasova, V.F. Anufrienko, *React. Kinet. Catal. Lett.* 10 (1979) 25–29.
- [51] T.P. Gorshkova, D.V. Tarasova, I.P. Olen'kova, G.N. Kustova, E.N. Yurchenko, T.A. Nikoro, *Kinet. Katal.* 25 (1984) 201–206.
- [52] Z. Liu, Y. Li, S. Qi, K. Xie, N. Wu, Q.X. Bao, *Appl. Catal.* 56 (1989) 207–218.
- [53] X. Wang, D.A. Vander Griend, J. Pless, P.C. Stair, K.R. Poepplmeier, Z. Hu, J.D. Jorgensen, *J. Alloys Compd.*, in press.
- [54] L.V. Kristallov, A.A. Fotiev, M.P. Tsvetkova, *Zh. Neorg. Khim.* 27 (1982) 3024–3029.
- [55] E.J. Baran, *Monatsh. Chem.* 106 (1975) 1–11.
- [56] I. Kanesaka, H. Hashiba, I. Matsuura, *J. Raman Spectrosc.* 19 (1988) 213–218.
- [57] W. Krasser, *Naturwissenschaften* 56 (1969) 213–214.
- [58] P.K. Dutta, R.E. Zaykoski, *Zeolites* 8 (1988) 179–182.
- [59] H. Jeziorowski, H. Knoezinger, *Chem. Phys. Lett.* 51 (1977) 519–522.
- [60] The references detailed in the introduction are oxygen deficient [36], oxygen rich [8,28,35], or stoichiometric [17].
- [61] A.W. Sleight, W.J. Linn, *Ann. N.Y. Acad. Sci.* 272 (1976) 22–44.
- [62] S. Fan, Q. Wang, B. Dou, Z. Yu, *Cuihua Xuebao* 12 (1991) 199–205.
- [63] T. Tsunoda, T. Hayakawa, T. Kameyama, K. Fukuda, K. Takehira, *J. Chem. Soc., Faraday Trans.* 91 (1995) 1125–1130.
- [64] J. Li, W. Song, B. Dou, *Yingyong Huaxue* 13 (1996) 58–60.
- [65] T. Shishido, T. Konishi, I. Matsuura, Y. Wang, K. Takaki, K. Takehira, *Catal. Today* 71 (2001) 77–82.
- [66] J.-M.M. Millet, J.C. Vedrine, *Top. Catal.* 15 (2001) 139–144.
- [67] W.M.H. Sachtler, N.H. de Boer, in: *3rd Proc. Intern. Congr. Catal.*, Amsterdam, 1964, 1965, p. 1, 252–263, discussion 263–255.
- [68] W.M.H. Sachtler, G.J.H. Dorgelo, J. Fahrenfort, R.J.H. Voorhoeve, in: *4th Proc. Intern. Congr. Catal.*, Moscow, 1968, 1970, p. 2, 604–627.
- [69] K. Chen, A.T. Bell, E. Iglesia, *J. Catal.* 209 (2002) 35–42.
- [70] Y.S. Yoon, K. Suzuki, T. Hayakawa, S. Hamakawa, T. Shishido, K. Takehira, *Catal. Lett.* 59 (1999) 165–172.
- [71] L.E. Briand, J.-M. Jehng, L. Cornaglia, A.M. Hirt, I.E. Wachs, *Catal. Today* 78 (2003) 257–268.
- [72] N.V. Porotnikov, O.A. Burnenko, T.I. Krosnenko, A.A. Fotiev, *Zh. Neorg. Khim.* 38 (1993) 1365–1368.
- [73] G. Busca, G. Ricchiardi, D.S.H. Sam, J.C. Volta, *J. Chem. Soc., Faraday Trans.* 90 (1994) 1161–1170.
- [74] A.S. Vuk, B. Orel, G. Drazic, P. Colomban, *Monatsh. Chem.* 133 (2002) 889–908.
- [75] C.T. Au, W.D. Zhang, H.L. Wan, *Catal. Lett.* 37 (1996) 241–246.
- [76] R. Kebabcioğlu, A. Mueller, *Chem. Phys. Lett.* 8 (1971) 59–62.
- [77] M.V. Ryzhkov, M.Y. Khodos, V.A. Gubanov, L.P. Benderskaya, N.M. Karablev, *Zh. Neorg. Khim.* 31 (1986) 1408–1412.
- [78] M.V. Ryzhkov, M.Y. Khodos, V.A. Gubanov, *Izvest. Akad. Neorg. Mater.* 24 (1988) 1530–1533.
- [79] V.I. Merkulov, J.S. Lannin, C.H. Munro, S.A. Asher, V.S. Veerasamy, W.I. Milne, *Phys. Rev. Lett.* 78 (1997) 4869–4872.
- [80] B. Racine, A.C. Ferrari, N.A. Morrison, I. Hutchings, W.I. Milne, J. Robertson, *J. Appl. Phys.* 90 (2001) 5002–5012.
- [81] M. Dubois, A. Naji, J.P. Buisson, B. Humbert, E. Grivei, D. Billaud, *Carbon* 38 (2000) 1411–1417.
- [82] S. Xie, E. Iglesia, A.T. Bell, *Langmuir* 16 (2000) 7162–7167.
- [83] P.J. Miller, *Spectrochim. Acta A* 27 (1971) 957–960.
- [84] M. Isaac, N. Santha, V.U. Nayar, *J. Raman Spectrosc.* 22 (1991) 237–239.
- [85] S.H. Kim, P.C. Stair, *Surf. Sci.* 457 (2000) L347–L353.
- [86] P.C. Stair, E. Weitz, *J. Opt. Soc. Am. B* 4 (1987) 255–260.
- [87] E.D. Palik, *Handbook of Optical Constants of Solids I*, Academic Press, New York, 1985;
E.D. Palik, *Handbook of Optical Constants of Solids II*, Academic Press, New York, 1991;
E.D. Palik, *Handbook of Optical Constants of Solids III*, Academic Press, New York, 1998.